

1 **Aeolus winds improve Arctic weather prediction**

2 **C.-C. Chou<sup>1</sup>, P. J. Kushner<sup>1</sup>, and Z. Mariani<sup>2</sup>**

3 <sup>1</sup>Department of Physics, University of Toronto, Toronto, M5S 1A7, Canada

4 <sup>2</sup>Meteorological Research Division, Environment and Climate Change Canada, Toronto, Canada

5 Corresponding author: Chih-Chun Chou ([gina.chou@mail.utoronto.ca](mailto:gina.chou@mail.utoronto.ca))

6 **Key Points:**

- 7 • Operational wind products are a key component of skillful numerical weather prediction
- 8 in the Arctic.
- 9 • Augmenting operational winds with Aeolus winds could enhance the forecasts of winds
- 10 and temperature fields by 14-18%.
- 11 • Aeolus wind improvements are most pronounced on strong wind days.

12 **Abstract**

13 It has been proven that assimilating winds from the Aeolus global Doppler wind lidar would  
14 enhance the predictive skill of weather forecast models. In this study, we use a series of  
15 Observing System Experiments to examine how operational winds and Aeolus winds impact  
16 Environment and Climate Change Canada’s global forecast system over the data-sparse Arctic  
17 region. Aeolus winds improve the tropospheric wind and temperature forecasts by about 0.7 to  
18 0.9% of error reduction (a 15-20% effect compared to the impact of operational wind products),  
19 while having little impact on the specific humidity field. In particular, Aeolus winds have an  
20 impact on forecasts of strong wind days on the wind and temperature fields that is double the  
21 impact of the forecasts of less intense wind days and provides a disproportionate improvement to  
22 forecasts on these days compared to other operational wind measurements. These findings  
23 suggest significant potential for global doppler wind lidar observations to enhance severe-  
24 weather prediction in polar regions.

25 **Plain Language Summary**

26 Wind observations are necessary to produce accurate weather forecasts. Aeolus is a new satellite  
27 that provides the first global wind profile measurements and it has a proven positive impact on  
28 forecasts. In this study, we investigate the impact of a large set of wind observations, including  
29 Aeolus winds, on Arctic weather forecasts using Canada’s main forecast. We can calculate how  
30 these wind observations improve the forecast throughout the atmosphere, and find that Aeolus  
31 winds further improve the forecast in the lower atmosphere. Furthermore, our findings highlight  
32 the heightened significance of wind observations in ensuring precise forecasts of strong wind  
33 days. The difference is about double the improvement on the forecast of less intense wind days.  
34 This suggests that future doppler wind lidar programs following from Aeolus could significantly

35 benefit forecast skill in data-sparse regions like the Arctic and Antarctic, which are of growing  
36 societal, political, and economic interest.

## 37 **1 Introduction**

38 Arctic weather forecasts produced by operational numerical weather prediction (NWP)  
39 models present unique challenges (Bauer et al., 2016; Jung et al., 2016; Gascard et al., 2017).  
40 The Arctic presents unique logistical and environmental challenges that hinder real-time data  
41 collection and the maintenance of observation equipment (Randriamampianina et al., 2019;  
42 Lawrence et al., 2019; James et al., 2020; Joe et al., 2020; Chou et al., 2020). Furthermore, the  
43 Arctic's unique geography and rapidly changing climate contribute to unpredictable and extreme  
44 weather events (Cohen et al. 2014; Francis et al., 2017; Lawrence et al., 2019; Eikeland et al.,  
45 2022). Nevertheless, improving Arctic forecasts remains imperative for the safety of residents  
46 and travellers in the region. Furthermore with melting sea ice opening up new opportunities, the  
47 Arctic is gaining increasing importance for shipping and industry (Gascard et al., 2017; Eicken,  
48 2013; Inoue et al., 2015). Finally, given implications of Arctic change for sea level rise and  
49 altered weather patterns, accurate forecasts promises to improve our understanding of and ability  
50 to adapt to climate change (Cohen et al. 2014; Jung et al., 2014; Overland et al. 2015; Francis et  
51 al., 2017; Laroche and Poan, 2021).

52 An essential element in producing reliable forecasts is the initialization of NWP systems  
53 with precise and timely observational data (Inoue et al., 2015; Randriamampianina et al., 2021).  
54 These observations allow estimation of the present atmospheric state, enabling the NWP system  
55 to establish the initial conditions necessary for accurate forecasts. Wind is a fundamental  
56 component of atmospheric dynamics, influencing the movement of air masses, the formation and  
57 evolution of weather systems, and the transport and advection of heat, moisture, and other

58 atmospheric constituents (Baker et al., 1995; Graham et al., 2000; Naakka et al., 2019). Thus,  
59 wind observations play a pivotal role in NWP initialization, even after accounting for the balance  
60 that constrains winds given pressure and temperature measurements (Horányi et al., 2014;  
61 Naakka et al., 2019; James et al., 2020).

62 Observations of altitude-resolved winds are available through aircraft reports (AMDAR;  
63 Dai et al., 2014; James et al., 2020), radiosondes (Durre et al., 2018; Carminati et al., 2019; Rani  
64 et al., 2021), and wind profiling technologies (e.g., Doppler radar and lidar; Augustine and  
65 Zipser, 1987; Rogers et al., 1993; Liu et al., 2020). However, these observations are often  
66 sporadic and notably scarce, particularly over vast bodies of water like oceans and the polar  
67 regions. Passive space-based observations offer an alternative, with Atmospheric Motion Vectors  
68 (AMVs) estimating wind speed and direction based on cloud and water vapor movements  
69 (Velden et al., 2017; Mizyak et al., 2016). Additionally, space-based scatterometers provide  
70 surface winds over the ocean. Despite the advantages of AMVs in offering wind information  
71 across multiple tropospheric layers through multispectral water vapor remote sensing (Velden et  
72 al., 1997; Bormann and Thépaut, 2004; Le Marshall et al., 2008), they lack precision in altitude  
73 assignment and are limited to a few levels, hindering their representation of small-scale vertical  
74 wind profile structures. Conversely, spaceborne scatterometers focus only on near-surface ocean  
75 winds, with their accuracy highly dependent upon surface weather conditions (Chiara et al.,  
76 2017; Young et al., 2017).

77 The Aeolus mission, featuring the first spaceborne Doppler Wind Lidar (DWL), provides  
78 the first-ever global horizontal line-of-sight (HLOS) wind profile measurements. Studies have  
79 demonstrated that assimilating Aeolus HLOS winds into NWP systems significantly enhances  
80 forecast accuracy. Examples of operational forecast systems include those of ECMWF (Rennie

81 et al., 2021), NCMRWF (George et al., 2021), DWD (Martin et al., 2023), NOAA (Garrett et al.,  
82 2022), Météo-France (Pourret et al., 2022), and Environment and Climate Change Canada  
83 (ECCC; Laroche and St-James, 2022). Most of the improvements were found in the tropical  
84 troposphere to lower stratosphere. Notably, Aeolus winds have also demonstrated a beneficial  
85 impact on forecasts in data-sparse regions such as the Southern Hemisphere extra-tropics and the  
86 Arctic (Mile et al., 2022; Chou and Kushner, 2023; Zuo and Hasager, 2023).

87         Despite the good coverage that polar-orbiting satellites provide over the Arctic, more  
88 than 90% of the assimilated observations over the Arctic are microwave and infrared radiances  
89 (Lawrence et al., 2019; Randriamampianina et al., 2021). As previously discussed, wind  
90 observations from conventional surface and aircraft measurements are extremely sparse in this  
91 region. Hence, it is important to assess the impact of existing wind observations and any  
92 additional wind observations over the Arctic to compare and determine their impact on NWP  
93 model performance over the Arctic.

94         In this study, we extend the work of Chou and Kushner (2023) and evaluate the impact of  
95 operational winds and Aeolus winds on the global forecast system of ECCC with a focus on the  
96 Arctic. Chou and Kushner (2023) used a series of Observing System Experiments (OSE), in  
97 which all operational winds or Aeolus winds are withheld in the assimilation and the forecasts  
98 are verified against the fifth-generation European Centre for Medium-Range Weather Forecasts  
99 (ECMWF) atmospheric reanalysis (ERA5, Hersbach et al., 2023). The integration of operational  
100 winds significantly enhanced tropospheric wind forecasts, particularly in tropical regions,  
101 resulting in an impressive 8% reduction in forecast error. Further augmenting these assimilations  
102 with Aeolus winds contributed an additional 0.7-0.9% improvement or about 10% of the impact  
103 of operational winds. Notably, Aeolus winds also proved beneficial in regions with limited data,

104 such as the Arctic and the extra-tropical Southern Hemisphere, demonstrating a reduction in  
105 forecast errors ranging from 0.5% to 0.9%. While operational winds contribute significantly to  
106 forecast improvement, unexpected occurrences such as the COVID-19 pandemic can disturb  
107 aircraft measurements, resulting in less precise forecasts during such periods (James et al., 2020).  
108 This circumstance, and the need to quantify Doppler wind lidar profiles' impact in isolation from  
109 other wind-observation systems, prompts the addition of this study's OSE labeled "CNTRL-  
110 wind+Aeolus" (refer to Section 2 for the experimental setup). This new OSE aims to specifically  
111 assess the isolated impact of Aeolus winds in the Arctic without the influence of other wind  
112 products.

113         Our investigation encompasses an assessment of the overall improvements in Arctic  
114 forecasts resulting from the assimilation of different sets of wind observations, as well as an  
115 exploration of the influence of wind observations on the forecasts related to enhanced kinetic  
116 energy and intense Integrated Vapor Transport (IVT). Henceforth, "disturbed" atmospheric state  
117 is used to describe days with strong winds or intense vapor transport. These two metrics were  
118 selected because of their large societal and economic impacts. Enhanced kinetic energy is  
119 commonly used as a severe-weather indicator, e.g. for severe storms, tornadoes, hurricanes, and  
120 typhoons (Palmén, 1958; DeMego and Bosart, 1982; Misra et al., 2013; Bass et al., 2017) and as  
121 an indirect indicator of extreme rainfall and flooding events (Brodie and Rosewell, 2007; Chang  
122 et al., 2017; Kim et al., 2022). Energetic systems can also transport substantial moisture from  
123 moisture sources, which can lead to weather-related water damage (Hills, 1978; Jiang, 2003;  
124 Chen et al., 2012; Martinez et al., 2019; Olaguera et al., 2021). Recent research suggests that  
125 ongoing climate changes are likely modifying IVT patterns, influencing the frequency and

126 intensity of future extreme weather events (Radic et al., 2015; Mattingly et al., 2016; Gershunov  
127 et al., 2017; Tan et al., 2019).

128 This paper is organized as follows: Section 2 outlines the experimental setup, including  
129 details on the ECCC global forecast system and OSE. In Section 3, we present impact scores by  
130 comparing forecasts to ERA5 and define strong wind and strong vapor transport events. Section  
131 4 unveils our results on the impact of wind observations on forecasts over the Arctic and on  
132 atmospheric events in the region. Finally, Section 5 offers a discussion of the main conclusions  
133 derived from this study.

## 134 **2 Experimental Setup**

135 OSEs are used to evaluate and assess the impact of observational data on NWP models  
136 by adding or removing a set of observations that are assimilated into the NWP model (Bouttier  
137 and Kelly, 2001; Laroche and Poan, 2021; Laroche and St-James, 2022). In this study, we use an  
138 extension of the series of OSEs used in Chou and Kushner (2023) to examine the impact of the  
139 operational wind observations and of Aeolus HLOS winds on the Arctic forecasts of the  
140 Canadian Global Deterministic Prediction System (GDPS). The OSEs cover two seasons: from  
141 July 1 to September 30 2019 (summer 2019) and from December 1 2019 to March 31 2020  
142 (winter 2020). The atmospheric component of the forecast system is the latest version of the  
143 operational Global Environmental Multiscale (GEM) model implemented at ECCC in 2019  
144 (McTaggart-Cowan et al., 2019) and the ocean component of the forecast system is the NEMO  
145 ocean model (Smith et al., 2018). The model uses approximately 15 km horizontal grid spacing  
146 and 84 vertical levels. The data assimilation scheme is the operational four-dimensional  
147 ensemble-variational (4D-EnVar) (Buehner et al., 2015) system, with a 6-h assimilation window  
148 which includes over 13 million observations assimilated daily. Two forecasts were generated

149 daily (at 00 and 12 UTC). To minimize the computational cost, a coarser horizontal grid  
150 resolution of 39 km is employed and some aspects of the GEM physics are simplified.  
151 Implications of the use of this coarse resolution will be discussed in Section 5. Further details  
152 and justification on this simplified GDPS version are provided in Laroche and St-James (2022)  
153 and Chou and Kushner (2023). To examine the impact of wind observations, four experiments  
154 are carried out:

- 155 1. CNTRL, an experiment with all operational observations.
- 156 2. CNTRL–winds (i.e., “control-minus-winds”), an experiment with all operational  
157 observations except the operational wind observations. Operational winds include wind  
158 measurements from AMDAR, AMVs, radiosondes, surface stations, surface buoys, wind  
159 profilers, and scatterometry. This assesses the impact of all operational wind products on  
160 NWP skill.
- 161 3. CNTRL–wind+ Aeolus (i.e., “control-minus-winds-plus-Aeolus”), an experiment with all  
162 operational observations and Aeolus HLOS winds (both Rayleigh-clear and Mie-cloudy  
163 winds) but without the operational wind observations. The winds used are from the  
164 second reprocessed product, the Level-2B11 product. This tests the impact of Aeolus  
165 winds in isolation from the other wind products and provides an assessment of NWP  
166 performance if traditional wind observations were halted (such as the reduction in  
167 AMDAR flights during Covid 19) but Aeolus was assimilated.
- 168 4. CNTRL+ Aeolus (i.e., “control plus Aeolus”), an experiment that adds the Aeolus HLOS  
169 winds (both Rayleigh-clear and Mie-cloudy winds) to the CNTRL experiment. This tests  
170 the impact of Aeolus winds on top of the other wind products and provides an assessment  
171 of NWP performance if Aeolus winds were operationally assimilated.



172 Chou and Kushner (2023) used OSEs 1, 2, and 4. The current study is the first to use OSE 3 to  
173 test the effect of Aeolus wind impacts separately from other wind products.

174 To evaluate the impact of the wind observations, we compare the forecast root-mean-  
175 square error (RMSE) between the experiments. The mathematical expression of the forecast  
176 impact scores will be discussed in Section 3. Henceforth, the expression “impact of operational  
177 winds” (IOW) refers to the normalized change in the forecast scores from the CNTRL compared  
178 to the CNTRL-winds (i.e., error of CNTRL-winds minus error of CNTRL, which is therefore  
179 positive for improvement), the expression “impact of Aeolus winds” (IAW) refers to the change  
180 in the forecast scores from the CNTRL-winds+Aeolus compared to the CNTRL-winds (i.e.,  
181 error of CNTRL-winds minus error of CNTRL-winds+Aeolus, which is therefore, again,  
182 positive for improvement), and the expression “impact of Aeolus on top of operational winds”  
183 (IAOW) refers to the change from the CNTRL+Aeolus compared to the CNTRL (i.e., error of  
184 CNTRL minus error of CNTRL+Aeolus, so, again, positive for improvement).

### 185 **3 Method**

186 We verify the forecasts from OSEs described in Section 2, against ERA5 from ECMWF  
187 (Hersbach et al., 2023). ERA5 is based on a four-dimensional variational (4DVar) data  
188 assimilation scheme using Cycle 41r2 of the Integrated Forecast System (IFS). We use the  
189 hourly winds, temperature, and specific humidity at 00 and 12 UTC. The data are gridded on a  
190 regular latitude-longitude grid of  $0.25^\circ$ , but linearly interpolated onto grid of  $0.5^\circ$  to match the  
191 coarser resolution of the OSEs, and only the OSEs’ 16 pressure levels are selected (10, 20, 30,  
192 50, 70, 100, 150, 200, 250, 300, 400, 500, 700, 850, 925, and 1000 hPa).

193 The impact of wind observations is defined as the normalized change (percentage  
194 change) in the forecast RMSE between the experiments over the Arctic. The steps to calculate  
195 the forecast RMSE are as follows:

- 196 1. Calculate the cosine-weighted mean-square-error (MSE) between the forecasts from  
197 OSEs and the verification field from ERA5, over the Arctic (70° to 90°N), for each  
198 forecast hour (two forecasts daily for a total of seven months). The MSE for a scalar field  
199  $x$  (i.e., temperature, specific humidity, and IVT) is

$$200 \quad MSE = \frac{\sum_i w_i (x_f - x_v)_i^2}{\sum_i w_i}$$

201 (1)

202 and the MSE for a vector field  $\vec{v}$  (i.e., vector wind and wind shear) is

$$203 \quad MSE_{vector} = \frac{\sum_i w_i \|\vec{v}_f - \vec{v}_v\|_i^2}{\sum_i w_i}$$

204 (2)

205 The index  $i$  indicates a grid point along a latitude band, the subscript  $f$  indicates the  
206 forecast, and the subscript  $v$  indicates the verification field. The weight  $w_i = \cos \theta_i$ ,  
207 where  $\theta_i$  is the latitude at location  $i$ .

- 208 2. The weighted MSEs are averaged over the seven months covering the available Aeolus  
209 observation products.
- 210 3. The square-root of the averaged weighted MSEs is the RMSE at each pressure level.
- 211 4. The normalized change in scores represents the percentage change of the RMSE between  
212 a pair of OSEs from Step 3.

213 5. The tropospheric impact score is the averaged scores from Step 4 from the four pressure  
214 levels: 850 hPa, 500 hPa, 250 hPa, and 100 hPa.

215 As introduced in Section 2, the impact of operational winds (IOW) is the percentage  
216 difference of forecast RMSE between CNTRL and CNTRL-winds; the impact of Aeolus winds  
217 (IAW) is the percentage difference of CNTRL-winds+Aeolus and CNTRL-winds; the impact of  
218 Aeolus on top of operational winds (IAOW) is the percentage difference of CNTRL+Aeolus and  
219 CNTRL.

220 Chou and Kushner (2023) show that adding Aeolus winds into data assimilation, which  
221 are the first global wind profile measurements, can improve the forecasts of the vertical structure  
222 of the wind field. We carry out this analysis in this study and will investigate the impact of wind  
223 observations on Arctic weather events on the tropospheric wind vector, temperature, wind shear  
224 (thermal-wind) vector (defined as the vector wind difference between 250 hPa and 850 hPa),  
225 specific humidity, and IVT. Analysis of specific humidity was included to help interpret the  
226 results of the IVT analysis.

227 For the second part of the paper (Section 4.2), we will discuss the impact of wind  
228 observations over the Arctic when the atmosphere is disturbed (i.e., strong kinetic energy or  
229 intense IVT). In preliminary work, we have investigated the impact of wind observations on  
230 localized events, such as strong wind events at radiosonde stations over the Arctic and forecasts  
231 along Aeolus swaths. This analysis is not shown in this study because, due to the short period of  
232 the Aeolus mission and the coarse resolution of the OSE forecasts, there were not many  
233 individual local events to average over, and we found that the OSEs had limited ability to resolve  
234 smaller-scale atmospheric features associated with severe Arctic weather such as polar lows.  
235 Instead, to investigate the impact of wind observations on predictability of extreme Arctic

236 weather events, we focus on days in which the atmosphere is strongly disturbed over the entire  
 237 Arctic. In particular, we examine the impact of wind observations on the forecasts of “strong”  
 238 500-hPa Kinetic Energy (KE500) days vs. “normal” KE500 days, and of strong IVT days vs.  
 239 normal IVT days over the Arctic. The KE500 ( $m^2 s^{-2}$ ) is

$$240 \quad KE500 = \frac{1}{2}(u^2 + v^2)$$

241 (3)

242 where  $u$  and  $v$  are the 500-hPa zonal and meridional wind components, respectively. The IVT  
 243 ( $kgm^{-1}s^{-1}$ ) is

$$244 \quad IVT = \sqrt{\left(\frac{1}{g} \int_{1000}^{300} qu dp\right)^2 + \left(\frac{1}{g} \int_{1000}^{300} qv dp\right)^2}$$

245 (4)

246 where  $g$  is the gravitational acceleration,  $q$  is the specific humidity,  $u$  and  $v$  are the zonal and  
 247 meridional winds, and the product of the specific humidity and the winds is integrated over 1000,  
 248 925, 850, 700, 500, 400, and 300 hPa (Cordeira and Ralph, 2020; Reynolds et al., 2022).

249 We define the strong KE500 days and strong IVT days in a similar way. First, we define  
 250 the threshold at each grid point as the 90<sup>th</sup> percentile of the local KE500 or the local IVT for the  
 251 summer season and the winter season separately. We record the number of grid points poleward  
 252 of 70°N that exceed this threshold and take the top 25% of this number for both seasons  
 253 combined to get “strong weather-event days” with more disturbed atmospheric conditions. Trial  
 254 and error suggests that this provides sufficient sampling to assess the impact of wind  
 255 observations on the forecasts (Section 4.2).

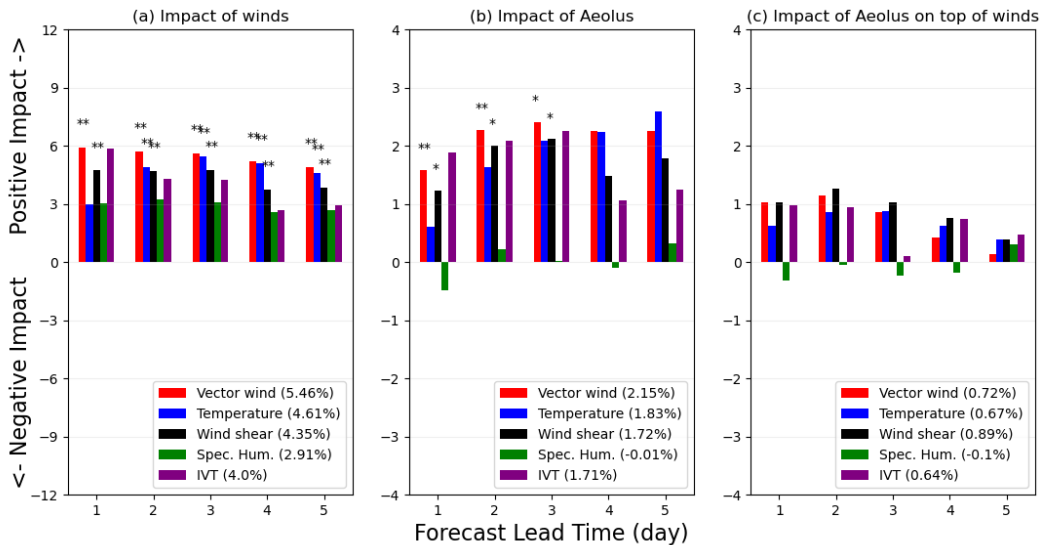
## 256 **4 Results**

### 257 4.1 Impact of operational winds and Aeolus winds over the Arctic

258 Figure 1 shows the impact of operational winds (IOW), Aeolus winds (IAW), and Aeolus  
259 winds on top of operational winds (IAOW) on the tropospheric forecast RMSE over the Arctic.  
260 Note that the y-axis extends from -12 to 12% for the IOW (panel a) and from -4 to 4% for the  
261 IAW and IAOW (Figure 1b,c). As expected, operational wind observations notably enhance the  
262 forecasts of wind fields (vector wind and wind shear) and the temperature field, which provides a  
263 context for assessing the impacts of Aeolus (Chou and Kushner, 2023). Averaged scores for  
264 these three fields over five days demonstrate an improvement of approximately 5%. Replacing  
265 operational winds by Aeolus winds, IAW (Figure 1b), consistently delivers a positive impact of  
266 about 2%, constituting roughly 40% of the improvement achieved with all operational winds. It  
267 is noteworthy that Aeolus, despite being a single-satellite measurement system, contributes  
268 meaningfully to forecast enhancement.

269 Considering all operational winds, as reflected in the IAOW in Figure 1c, Aeolus winds  
270 further enhance the wind and temperature fields throughout the five-day forecast lead time by  
271 0.7% and 0.9%, respectively, representing 14% to 18% of the overall improvement obtained with  
272 all operational winds. While this positive IAOW is relatively modest compared to improvements  
273 found by Aeolus for other models (e.g., Garrett et al., 2022; Rennie et al., 2021), it aligns with  
274 previous findings in OSEs conducted with the ECCO GDPS (Laroche and St-James, 2022; Chou  
275 and Kushner, 2023). The reasons for this modest impact are elaborated on in Chou and Kushner  
276 (2023). Despite the relatively small contribution, the impact of Aeolus winds on top of  
277 operational winds is noteworthy, particularly considering that Aeolus observations for this period  
278 constitute less than 1% of all operational wind observations. Notably, operational winds,

279 inclusive of measurements from various ground-based instruments, radiosondes, and satellites,  
 280 account for roughly 10% of all operational observations over the Arctic in the ECCC GDPS. The  
 281 lack of significance when assimilating Aeolus winds on top of operational winds might arise  
 282 from the simplification and relatively coarse resolution of the ECCC model version used in this  
 283 work to reduce computational cost, systematic model issues beyond this simplification, or  
 284 assimilation system deficiencies, as discussed in Chou and Kushner (2023). Importantly, the  
 285 IAW remains significant, reaching at least 90% confidence level, particularly in the wind fields  
 286 for the first three days of the lead time.



287  
 288 Figure 1: Normalized change in RMS forecast error between (a) CNTRL–winds and CNTRL (IOW), (b) CNTRL–  
 289 winds and CNTRL–winds+Aeolus (IAW), and (c) CNTRL and CNTRL+Aeolus (IAOW), compared to ERA5 in the  
 290 troposphere for vector wind (red), temperature (blue), wind shear (black), specific humidity (green), and integrated  
 291 vapor transport (IVT) (purple) in the troposphere (850-100hPa layer) for 5-day forecasts over the Arctic. Positive  
 292 impact means a reduction in the forecast error. The impacts that are significant at 95% confident level are marked  
 293 with double asterisk (\*\*) and impacts that are significant at 90% confident level are marked with single asterisk (\*).  
 294 The significance is tested using a t-test for the null hypothesis that the pair of experiments have identical cosine-

295 weighted RMSE from all four layers. The averaged impact over the five forecast lead time days is shown in the  
296 brackets.

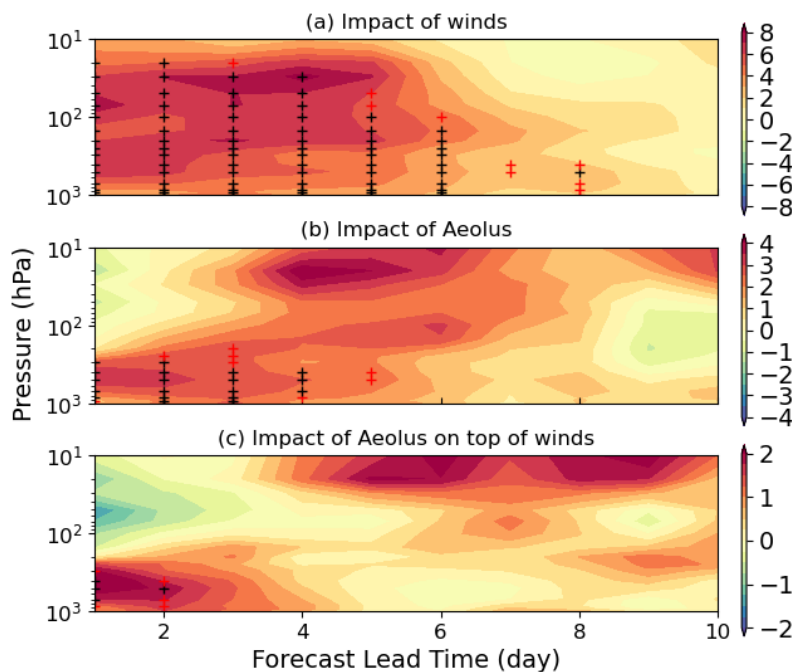
297 Both operational winds and Aeolus winds show minimal to no impact on the specific  
298 humidity field, despite enhancements in other fields. The averaged IOW in Figure 1a over a five-  
299 day forecast lead time is approximately 3%, which is about half of the impact observed in the  
300 vector wind field. The IAW in Figure 1b and the IAOW in Figure 1c on the specific humidity  
301 field lack consistency throughout the forecast lead time. Consequently, the impact on the IVT,  
302 encompassing both wind and specific humidity information, falls between the impact on the  
303 wind fields and the specific humidity field. The averaged scores for the IVT are 4.0, 1.7, and  
304 0.6% for the IOW, IAW, and IAOW, respectively.

305 Figure 2 provides a view of the spatial structure of the impact of wind observations on the  
306 vector wind field by breaking down the pressure-level and forecast lead time dependence (up to  
307 day 10). The tropospheric impacts observed in the first five days of the forecast lead time align  
308 with the findings depicted in Figure 1. Note that the color scale is compressed by factors of two  
309 when transitioning from the IOW in Figure 2a to the IAW in Figure 2b, and to the IAOW in  
310 Figure 2c. This demonstrates, consistently with Figure 1, that IAW contributes to about half of  
311 the improvement obtained by all operational winds. In the case of tropospheric IAOW, the  
312 enhancements from Aeolus winds on top of operational winds exceed 25% of the improvement  
313 obtained with all operational winds in short-range forecasts and are slightly less than 20% in  
314 short- to medium-range forecasts.

315 Conversely, Figure 2 reveals a degradation in forecast skills when assimilating Aeolus in  
316 the stratosphere. As previously discussed in Chou and Kushner (2023), this issue may arise from

317 the simplification of the ECCO model version used to reduce computational costs, systematic  
318 model issues beyond this simplification, or deficiencies in the assimilation system.

319 Overall, Figure 2 underscores the potential of Aeolus to enhance medium- to long-range  
320 forecasts, particularly in the upper atmosphere beyond day 4. The IAW accounts for more than  
321 50% of the improvements from operational winds, and more than 25% for the IAOW. This  
322 stratospheric improvement in long-range forecasts over the Arctic is primarily attributed to the  
323 signal during the winter season, characterized by an anomalously strong Arctic stratospheric  
324 polar vortex in 2019-2020 (Chou and Kushner, 2023; Lawrence et al., 2020).



325

326 Figure 2: Normalized change in RMS forecast error as a function of pressure level between (a) CNTRL–winds and  
327 CNTRL, (b) CNTRL–winds and CNTRL–winds+Aeolus, and (c) CNTRL and CNTRL+Aeolus, for wind vector for  
328 10-day forecasts over the Arctic. Positive impact means a reduction in the forecast error. The impacts that are  
329 significant at 95% confident level are marked with black plus sign and impacts that are significant at 90% confident



330 level are marked with red plus sign. The scores with respect to ERA5 data are interpolated onto the 16 pressure  
331 levels of the OSEs.

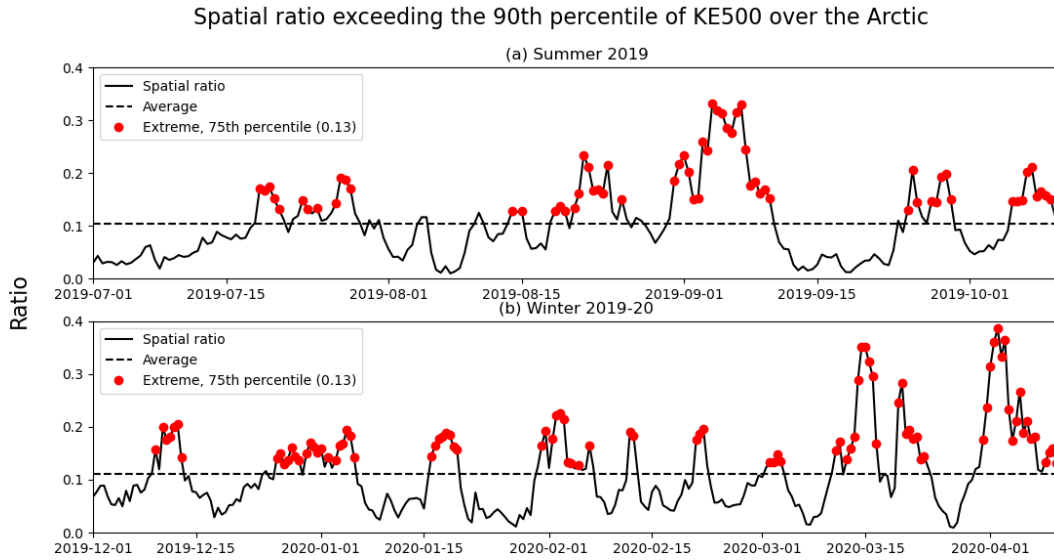
332           Despite previous challenges in attributing improvements in the Arctic forecast to  
333 localized regions, some regional insight can be gained by including all forecasts and dividing the  
334 Arctic into quadrants. We repeat the pan-Arctic analysis for four Arctic quadrants and investigate  
335 the IOW, IAW, and IAOW on the wind and temperature fields over each quadrant (SFigures 1 to  
336 3 respectively). This shows that over the Arctic, Russian-Pacific-Northern Canada sector  
337 forecasts ( $90^{\circ}\text{E} - 180^{\circ}\text{E}$  and  $180^{\circ}\text{E} - 270^{\circ}\text{E}$ ) are most improved and sensitive to the wind  
338 observations; the IOW on the vector wind field are 5.7% and 6.7%, compared to 4.6% and 5.0%  
339 over the other two quadrants and similar results are found when Aeolus winds are assimilated.  
340 The IAW and IAOW on the vector wind field are around 2.7 and 0.8% respectively over the  
341 quadrants between  $90^{\circ}$  and  $270^{\circ}\text{E}$ , which are about 40 and 13% of the IOW, but the impacts are  
342 only around 1.6 and 0.6% over the other two quadrants, which are 33 and 12% compared to  
343 IOW. The reason why this region's forecasts are more sensitive to wind observations remains  
344 unclear, but it is consistent when different sets of wind observations are assimilated into the  
345 forecast model. There are many aspects that can lead to this difference; for example, the  
346 proportion of land, ocean, and snow/ice, number of observations over the region, and the physics  
347 used for the region in the model. However, such investigations are beyond the scope of this  
348 paper.

349

#### 350 4.2 Impact of wind observations on strong wind and vapor transport events over the Arctic

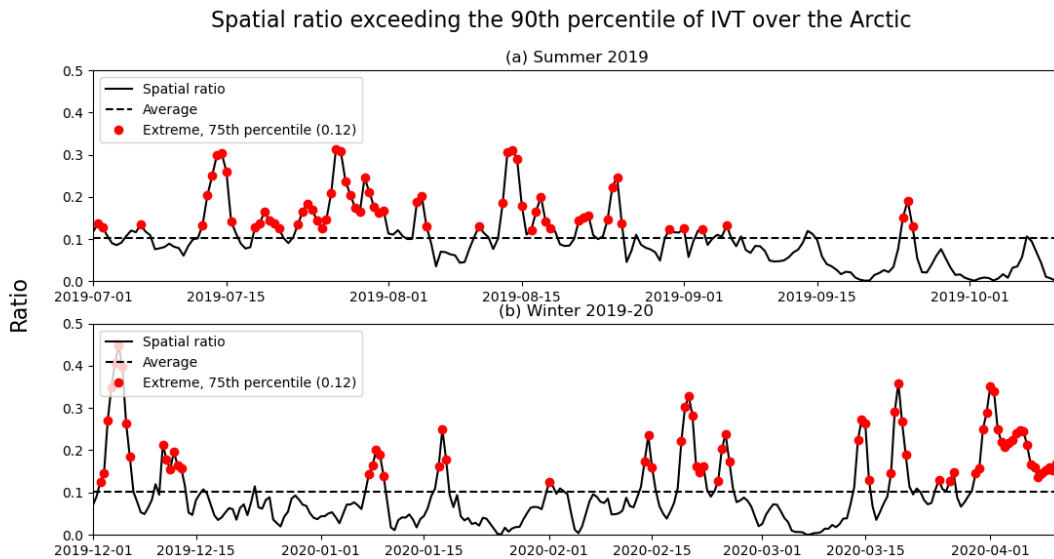
351           We are interested in whether wind observations would improve the forecasts of severe  
352 weather events and how much in advance the forecasts would show an improvement. More

353 specifically, this subsection presents the impact of wind observations on strong wind events and  
354 water vapor transport events over the Arctic. The proportions of the Arctic that exceed the  
355 KE500 and IVT thresholds (90<sup>th</sup> percentile of the field of the season) are recorded at each  
356 forecast hour and the time-series of this spatial coverage ratio are shown in Figures 3 and 4,  
357 respectively. The days that are defined as more energized or in a more disturbed atmospheric  
358 state are the top 25% (red dots) of this spatial coverage ratio during the entire period of analysis.  
359 For these events at and above the 75<sup>th</sup> percentile, the forecasts that are defined as strong KE500  
360 occur when at least 13% of the Arctic points exceed the thresholds of the field, and the forecasts  
361 that are defined as strong IVT occur when at least 12% of the Arctic exceed the threshold of the  
362 field. Strong KE500 forecasts do not necessarily overlap with the forecasts that have strong IVT.  
363 For example, before mid-July 2019, there are around eight forecasts that experienced strong IVT,  
364 but none of the forecasts during this period are defined as strong KE500 forecasts. Also, at the  
365 end of December 2019 and in early January 2020, most of the forecasts show an energetic, strong  
366 KE500, atmosphere, but the IVT over the Arctic during this period is relatively weak. By  
367 grouping the forecasts using the top 25%, we get sufficient forecasts (around 100 forecasts) to  
368 compare and to investigate the impact of wind observations on disturbed atmospheric states.



369

370 Figure 3: The time-series (solid black line) during (a) summer 2019 and (b) winter 2019-20 of the spatial coverage  
 371 ratio that exceeds the 90<sup>th</sup> percentile of the 500-hPa Kinetic Energy of the season over the Arctic. The time-averaged  
 372 of the spatial ratio of the season is shown as the dashed black line. The strong KE500 days (red dots) are defined as  
 373 when the spatial ratio exceeds the 75<sup>th</sup> percentile of the two seasons combined. The threshold of the spatial ratio (the  
 374 75<sup>th</sup> percentile) is indicated in the legend for the extreme days.

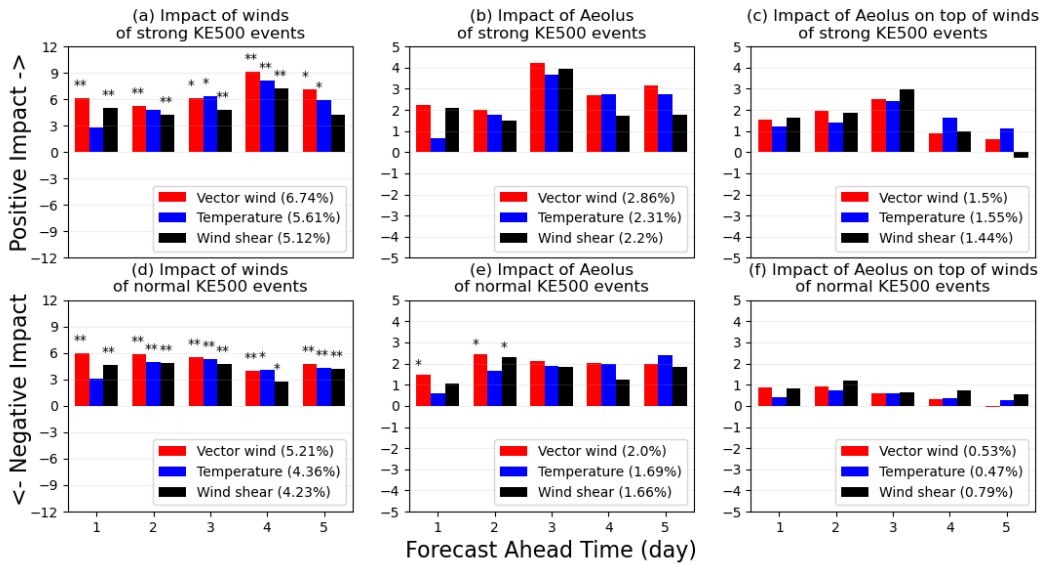


375

376 Figure 4: Similar to Figure 3, but for the spatial coverage ratio that exceeds the 90<sup>th</sup> percentile of the IVT over the  
377 Arctic.

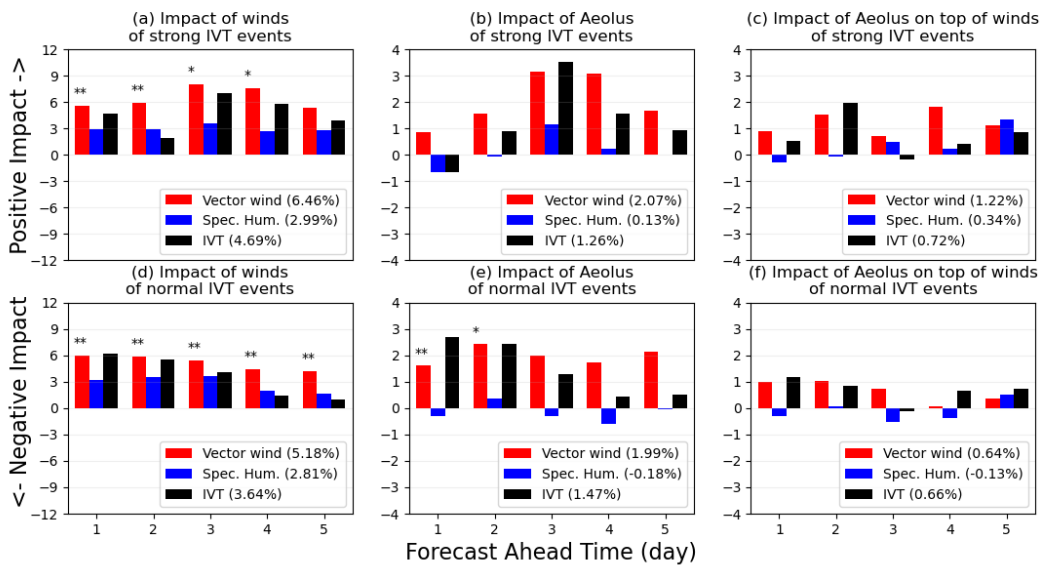
378 We use the same approach, outlined in Section 3, to find the normalized change in the  
379 forecast RMSE between a pair of experiments, but we composite tropospheric forecast skill  
380 impacts conditioned on strong (Figure 5a,b,c) and normal (Figure 5d,e,f) Arctic KE500, and on  
381 strong (Figure 6a,b,c) and normal (Figure 6d,e,f) Arctic IVT. Note that the x-axis is showing the  
382 forecast “ahead” time, instead of the forecast lead time as shown in Figures 1 and 2. The forecast  
383 ahead time represents the number of days prior to the identified disturbed atmospheric day, as  
384 measured with KE500 or IVT. For instance, if there is a strong wind event on July 15<sup>th</sup>, then the  
385 scores show the impact of wind observations on forecasts of July 15<sup>th</sup> that were made prior to the  
386 event. If the score for forecasts of two-day ahead time is 2%, then it means that the forecast  
387 RMSE with two-day lead time that was made on July 13<sup>th</sup> is reduced by 2% when wind  
388 observations are assimilated.

389 The wind observations consistently provide more positive impact on forecasts of strong  
390 KE500 on wind and temperature fields. For example, the IOW on forecasts of normal KE500 is  
391 around 4.6% and it increases to around 5.8% when conditioned on forecasts of strong KE500.  
392 Consistent findings are noted with the assimilation of Aeolus winds. The impact scores show an  
393 increase from 1.8 to 2.4% when operational winds are replaced by Aeolus winds, when  
394 conditioned on normal (Figure 5e) and strong (Figure 5b) KE500 days. Specifically, the IAOW  
395 for forecasts of strong KE500 is nearly triple the impact scores observed when conditioned on  
396 normal KE500 days. The averaged scores over the five forecast lead times rise from 0.6 to 1.5%.



397

398 Figure 5: Normalized change in RMS forecast error for IOW (left column), IAW (middle column), and IAOW (right  
 399 column) for vector winds, temperature and wind shear, as a function of “Forecast Ahead Time” (see text), for strong  
 400 KE500 forecasts only (top row) and normal KE500 forecasts only (bottom row). Note that the scale of the y-axis  
 401 extends from -5 to 5% for panels b, c, e, and f. Significance testing as in Figure 1. Strong KE500 events are defined  
 402 in Figure 3; the remaining KE500 events are identified as “normal”.



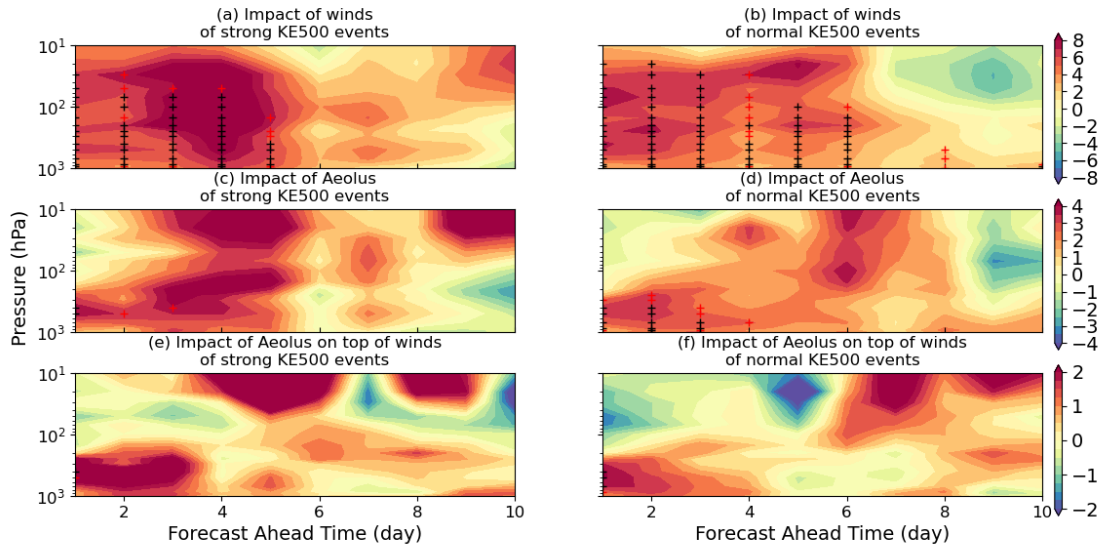
403

404 Figure 6: Similar to Figure 5, but for vector winds, specific humidity, and IVT, for strong and normal IVT events  
405 defined in Figure 4.

406 Greater impacts are also seen when conditioned on forecasts of strong IVT (Figure  
407 6a,b,c) compared to forecasts of normal IVT (Figure 6d,e,f). The IOW on the wind field  
408 increases by approximately 1.3% when conditioned on strong IVT and by 1.0% for the IVT field.  
409 Conversely, the averaged IAW over five days shows little to no difference when conditioned on  
410 forecasts of strong IVT days (Figure 6b,e). The impact scores averaged over the five forecast  
411 lead times on the wind and IVT fields exhibit no more than a 0.2% difference. If Aeolus winds  
412 are assimilated on top of operational winds, the IAOW would approximately double the impact  
413 scores for the wind field when conditioned on forecasts of strong IVT (Figure 6c). Generally,  
414 Aeolus winds (Figure 6b,c,e,f) demonstrate little to no consistent impact on the specific humidity  
415 field.

416 The results from Figure 5 encourage us to investigate the profiles of impact of wind  
417 observations conditioned on strong (Figure 7a,c,e) and normal (Figure 7b,d,f) Arctic KE500 with  
418 a longer forecast ahead time. Profiles of impact conditioned on strong and normal Arctic IVT are  
419 shown in the supplementary information (SFigure 6). The operational winds reduce the forecast  
420 RMSE by more than 8% throughout the atmosphere with 3 to 5 days of lead time before strong  
421 KE500 days (Figure 7a), whereas they only reduce the forecast RMSE by about 4% for normal  
422 KE500 (Figure 7b). When operational winds are replaced by Aeolus winds, the IAW on forecasts  
423 of strong KE500 with a lead time of 3 to 5 days (Figure 7c) accounts for approximately 50% of  
424 the improvement obtained with all operational winds. Consistently with our findings above, the  
425 IAW is about 40% of the IOW and the IAW impact on strong KE500 days is greater than on  
426 normal KE500 days (Figures 7c-d), and IAOW is about 25% of the IOW, with extended lower

427 tropospheric impacts four or more days ahead being evident for the strong KE500 days, which is  
428 not as evident for the normal KE500 days (Figures 7e-f).



429  
430 Figure 7: Normalized change in RMS forecast error as a function of pressure level for IOW (top row), IAW (middle  
431 row) and IAOW (bottom row), for wind vector errors up to 10 forecast days ahead. Positive impact means a  
432 reduction in the forecast error. The left column shows the impact of the added wind observations respectively of the  
433 strong KE500 days only defined in Figure 3 and column two shows the impact of the non-strong KE500 days only.  
434 Significance testing as in Figure 2.

## 435 5 Conclusions

436 The Arctic has fewer weather observation stations and limited data sources due to its low  
437 population density, limited accessibility, and harsh environment. However, the Arctic's  
438 distinctive geography, increasing economic activity, global geopolitical importance, and rapidly  
439 evolving climate changes necessitate advances in weather modeling and forecasting. Precise  
440 weather predictions in the Arctic are crucial for the safety of individuals and navigation in the  
441 area, and a deeper comprehension of Arctic weather has the potential to improve global climate  
442 models.

443 To better understand the role of wind observations in the weather forecasts over the  
444 Arctic, we have assessed the impact of operational winds (IOW), Aeolus winds (IAW), and  
445 Aeolus winds on top of operational winds (IAOW) on the ECCO global forecast system over the  
446 Arctic during July to September 2019 and December 2019 to March 2020. The analysis covers  
447 both the difference between disturbed atmospheric conditions (high versus normal KE500 and  
448 IVT days) and surveys different Arctic sectors for improvements. This extends Chou and  
449 Kushner (2023) who examined the general scale dependence and global distribution of IOW and  
450 IAOW. The IAOW has been enabled by the new experiment without the operational winds but  
451 with the Aeolus winds (CNTRL\_winds+Aeolus), which allows us to study the impact of Aeolus  
452 winds as if it were, hypothetically, the only source of wind observations.

453 As anticipated, operational winds significantly enhance Arctic forecasts, reducing  
454 forecast RMSE by approximately 5%, particularly in the wind and temperature fields. This  
455 improvement is even greater for disturbed atmospheric conditions, as measured by high KE500  
456 and IVT values. This highlights how wind observations become even more important during  
457 extreme atmospheric states where simple dynamical balances that couple mass and circulation  
458 break down. Despite Aeolus winds representing less than 1% of operational wind observations,  
459 substituting operational winds with Aeolus winds in the assimilation process results in an  
460 observed 2% reduction in errors, equivalent to approximately 40% of the improvement achieved  
461 by operational winds. This improvement extends to the additional forecast improvements seen on  
462 strong KE500 and IVT days. Thus, despite being derived from a single satellite, Aeolus winds  
463 can match nearly half of the forecast enhancement realized by operational winds, which  
464 incorporate wind measurements from multiple ground-based instruments, radiosondes, and  
465 satellites. This suggests that Doppler wind lidar systems have the potential to strongly



466 complement conventional wind observations. This was already seen when Aeolus data was  
467 shown, during the COVID-19 pandemic, to be capable of compensating for the disruption of  
468 AMDAR aircraft wind measurements and consequent forecast degradation (James et al., 2020).  
469 Altogether, assimilating Aeolus winds on top of operational winds (IAOW) yields an additional  
470 0.8% reduction in errors, constituting around 16% of the overall improvement obtained with all  
471 operational winds.

472         While wind observations exhibit positive outcomes for mass-related fields like  
473 temperature, operational winds only contribute approximately half of the impact on the specific  
474 humidity field compared to the temperature field. Additionally, both the IAW and IAOW show  
475 little to no influence on the specific humidity field over the Arctic. This suggests that wind  
476 observations have limited efficacy in improving the specific humidity field.

477         As noted, Aeolus not only improves overall forecasts over the Arctic but also improves  
478 predictions for specific days characterized by strong winds and enhanced water vapor transport,  
479 which are associated with extreme weather events. In particular, the IAOW further reveals a two  
480 to threefold increase in impact scores (ranging from 0.5 to 1.5% for strong KE500 and 0.6 to  
481 1.2% for intense IVT) on the wind field when forecasts are conditioned on a disturbed  
482 atmosphere, as opposed to normal days. While these results are found consistently in our  
483 diagnostics, their statistical significance is marginal and, we expect, will depend strongly on the  
484 smaller scale phenomena associated with extreme wind and IVT events. We thus strongly  
485 recommend conducting longer periods of OSEs at a higher resolution or with the use of a limited  
486 area regional forecast model.

487         The results also provide a compelling rationale for ECCO and other modelling centres to  
488 consider the operational assimilation of Aeolus winds. In particular, results have demonstrated

489 enhancements in forecast skill over data-sparse regions such as the Canadian Arctic, and for  
490 forecasts of intense wind events linked to extreme weather patterns, which can have large health,  
491 societal, and economic impacts. Notably, several European weather forecast centers, including  
492 ECMWF, DWD, Météo-France, and UK Met Office, have already embraced assimilation of  
493 Aeolus (Rennie et al., 2021; Pourret et al., 2022; Kiriakidis et al., 2023). Therefore, we  
494 recommend that weather forecast centers consider assimilating global wind profile measurements  
495 from the potential Aeolus follow-on mission, Aeolus-2, scheduled for launch in 2030 (Heliere et  
496 al., 2023).

497

#### 498 **Acknowledgments**

499 We thank Stéphane Laroche from ECCC for the Observing System Experiments, and the  
500 ECMWF for the ERA5 data. We were supported by the Canadian Space Agency's Earth System  
501 Science Data Analysis program.

502

#### 503 **Data availability**

504 The OSEs used in this paper can be provided by the corresponding author  
505 (gina.chou@mail.utoronto.ca) upon reasonable request. The ERA5 data can be downloaded from  
506 the Copernicus Climate Change Service (C3S) Climate Data Store  
507 (<https://doi.org/10.24381/cds.bd0915c6>, Hersbach et al., 2023).

508

509

510 **References**

- 511 Augustine, J. A., & Zipser, E. J. (1987). The Use of Wind Profilers in a Mesoscale  
512 Experiment. *Bulletin of the American Meteorological Society*, 68(1), 4-  
513 17. [https://doi.org/10.1175/1520-0477\(1987\)068<0004:TUOWPI>2.0.CO;2](https://doi.org/10.1175/1520-0477(1987)068<0004:TUOWPI>2.0.CO;2)
- 514 Baker, W. E., Emmitt, G. D., Robertson, F., Atlas, R. M., Molinari, J. E., Bowdle, D. A., Paegle,  
515 J., Hardesty, R. M., Menzies, R. T., Krishnamurti, T. N., Brown, R. A., Post, M. J.,  
516 Anderson, J. R., Lorenc, A. C., & McElroy, J. (1995). Lidar-Measured Winds from  
517 Space: A Key Component for Weather and Climate Prediction. *Bulletin of the American*  
518 *Meteorological Society*, 76(6), 869-888. [https://doi.org/10.1175/1520-  
519 0477\(1995\)076<0869:LMWFSA>2.0.CO;2](https://doi.org/10.1175/1520-0477(1995)076<0869:LMWFSA>2.0.CO;2)
- 520 Bass, B., Irza, J.N., Proft, J. *et al.* (2017). Fidelity of the integrated kinetic energy factor as an  
521 indicator of storm surge impacts. *Nat Hazards* **85**, 575–595.  
522 <https://doi.org/10.1007/s11069-016-2587-3>
- 523 Bauer, P., Magnusson, L., Thépaut, J.-N. and Hamill, T.M. (2016), Aspects of ECMWF model  
524 performance in polar areas. *Q.J.R. Meteorol. Soc.*, 142: 583-596.  
525 <https://doi.org/10.1002/qj.2449>
- 526 Bormann, N., & Thépaut, J.-N. (2004). Impact of MODIS polar winds in ECMWF's 4D-VAR  
527 data assimilation system. *Monthly Weather Review*, 132, 929–940.
- 528 Bouttier, F. and Kelly, G. (2001), Observing-system experiments in the ECMWF 4D-Var data  
529 assimilation system. *Quarterly Journal of the Royal Meteorological Society*, 127: 1469-  
530 1488. <https://doi.org/10.1002/qj.49712757419>

531 Brodie, I. and Rosewell, C. (2007). Theoretical relationships between rainfall intensity and  
532 kinetic energy variants associated with stormwater particle washoff. *Journal of*  
533 *Hydrology*, Volume 340, Issues 1–2, 2007, Pages 40-47, ISSN 0022-1694.  
534 <https://doi.org/10.1016/j.jhydrol.2007.03.019>

535 Buehner, M., McTaggart-Cowan, R., Beaulne, A., Charette, C., Garand, L., Heilliette, S.,  
536 Lapalme, E., Laroche, S., Macpherson, S. R., Morneau, J., & Zadra, A. (2015).  
537 Implementation of Deterministic Weather Forecasting Systems Based on Ensemble–  
538 Variational Data Assimilation at Environment Canada. Part I: The Global  
539 System. *Monthly Weather Review*, 143(7), 2532-2559. [https://doi.org/10.1175/MWR-D-](https://doi.org/10.1175/MWR-D-14-00354.1)  
540 [14-00354.1](https://doi.org/10.1175/MWR-D-14-00354.1)

541 Carminati, F., A. Migliorini, S., Ingleby, B., Bell, W., Lawrence, H., Newman, S., Hocking, J., &  
542 Smith, A. (2019). Using reference radiosondes to characterise NWP model uncertainty  
543 for improved satellite calibration and validation. *Atmospheric Measurement*  
544 *Techniques*, 12(1), 83-106.

545 Chang, J.-M., Chen, H., Jou, J.-D., Tsou, N.-C., and Lin, G.-W. (2017). Characteristics of  
546 rainfall intensity, duration, and kinetic energy for landslide triggering in Taiwan.  
547 *Engineering Geology*, Volume 231, Pages 81-87, ISSN 0013-7952.  
548 <https://doi.org/10.1016/j.enggeo.2017.10.006>

549 Chen, C.-S., Lin, Y.-L., Zeng, H.-T., Chen, C.-Y., and Liu, C.-L. (2012). Orographic effects on  
550 heavy rainfall events over northeastern Taiwan during the northeasterly monsoon season.  
551 *Atmospheric Research*, Volume 122, 2013, Pages 310-335, ISSN 0169-8095.  
552 <https://doi.org/10.1016/j.atmosres.2012.10.008>

553 Chiara, G. D., Bonavita, M., & English, S. J. (2017). Improving the Assimilation of  
554 Scatterometer Wind Observations in Global NWP. *IEEE Journal of Selected Topics in*  
555 *Applied Earth Observations and Remote Sensing*, 10(5), 2415-2423.  
556 <https://doi.org/10.1109/JSTARS.2017.2691011>

557 Chou, C.-C. & Kushner, P.J. (2023) Scale-dependent impact of *Aeolus* winds on a global forecast  
558 system. *Quarterly Journal of the Royal Meteorological Society*, 1–15.  
559 <https://doi.org/10.1002/qj.4601>

560 Chou, C.-C., Kushner, P. J., Laroche, S., Mariani, Z., Rodriguez, P., Melo, S., and  
561 Fletcher, C. G.: Validation of the Aeolus Level-2B wind product over Northern Canada  
562 and the Arctic, *Atmos. Meas. Tech.*, 15, 4443–4461, [https://doi.org/10.5194/amt-15-](https://doi.org/10.5194/amt-15-4443-2022)  
563 [4443-2022](https://doi.org/10.5194/amt-15-4443-2022)

564 Cohen, J., Screen, J., Furtado, J. *et al.* (2014). Recent Arctic amplification and extreme mid-  
565 latitude weather. *Nature Geosci* **7**, 627–637. <https://doi.org/10.1038/ngeo2234>

566 Cordeira, J. M., & Ralph, F. M. (2021). A Summary of GFS Ensemble Integrated Water Vapor  
567 Transport Forecasts and Skill along the U.S. West Coast during Water Years 2017–  
568 20. *Weather and Forecasting*, 36(2), 361-377. <https://doi.org/10.1175/WAF-D-20-0121.1>

569 Dai, C., Wang, Q., Kalogiros, J. A., Lenschow, D. H., Gao, Z., & Zhou, M. (2014). Determining  
570 boundary-layer height from aircraft measurements. *Boundary-layer meteorology*, 152,  
571 277-302.

572 DiMego, G. J., & Bosart, L. F. (1982). The Transformation of Tropical Storm Agnes into an  
573 Extratropical Cyclone. Part II: Moisture, Vorticity and Kinetic Energy Budgets. *Monthly*

574 *Weather Review*, 110(5), 412-433. <https://doi.org/10.1175/1520->  
575 [0493\(1982\)110<0412:TTOTSA>2.0.CO;2](https://doi.org/10.1175/1520-0493(1982)110<0412:TTOTSA>2.0.CO;2)

576 Durre, I., Yin, X., Vose, R. S., Applequist, S., & Arnfield, J. (2018). Enhancing the Data  
577 Coverage in the Integrated Global Radiosonde Archive. *Journal of Atmospheric and*  
578 *Oceanic Technology*, 35(9), 1753-1770. <https://doi.org/10.1175/JTECH-D-17-0223.1>

579 Eicken, H. (2013). Arctic sea ice needs better forecasts. *Nature*, 497(7450), 431-433.

580 Eikeland, O. F., Hovem, F. D., Olsen, T. E., Chiesa, M., Bianchi, F. M. (2022). Probabilistic  
581 forecasts of wind power generation in regions with complex topography using deep  
582 learning methods: An Arctic case. *Energy Conversion and Management: X*, Volume 15,  
583 2022, 100239, ISSN 2590-1745. <https://doi.org/10.1016/j.ecmx.2022.100239>

584 Francis, J.A., Vavrus, S.J. and Cohen, J. (2017), Amplified Arctic warming and mid-latitude  
585 weather: new perspectives on emerging connections. *WIREs Clim Change*, 8: e474.  
586 <https://doi.org/10.1002/wcc.474>

587 Garrett, K., Liu, H., Ide, K., Hoffman, R.N. & Lukens, K.E. (2022). Optimization and impact  
588 assessment of Aeolus HLOS wind assimilation in NOAA's global forecast  
589 system. *Quarterly Journal of the Royal Meteorological Society*, 148(747), 2703–2716.  
590 <https://doi.org/10.1002/qj.4331>

591 Gascard, J.C., Riemann-Campe, K., Gerdes, R. *et al.* (2017). Future sea ice conditions and  
592 weather forecasts in the Arctic: Implications for Arctic shipping. *Ambio* **46** (Suppl 3),  
593 355–367. <https://doi.org/10.1007/s13280-017-0951-5>

594 George, G., Halloran, G., Kumar, S., Rani, S. I., Bushair, M.T., Jangid, B. P., George, J. P., and  
595 Maycock, A. (2021). Impact of Aeolus Horizontal Line of Sight Wind Observations in a

596 Global NWP System” *Atmospheric Research* 261 (October): 105742.  
597 <https://doi.org/10.1016/j.atmosres.2021.105742>

598 Gershunov, A., Shulgina, T., Ralph, F. M., Lavers, D. A., and Rutz, J. J. (2017), Assessing the  
599 climate-scale variability of atmospheric rivers affecting western North  
600 America, *Geophysical Research Letter.*, 44, 7900–7908, doi:[10.1002/2017GL074175](https://doi.org/10.1002/2017GL074175).

601 Graham, R.J., Anderson, S.R. and Bader, M.J. (2000), The relative utility of current observation  
602 systems to global-scale NWP forecasts. *Quarterly Journal of the Royal Meteorological*  
603 *Society*, 126: 2435-2460. <https://doi.org/10.1002/qj.49712656805>

604 Heliere, A., Wernham, D., Mason, G., De Villele, G., Corselle, B., Lecrenier, O., Belhadj, T.,  
605 Bravetti, P., Arnaud, S., Bon, D., Lingot, P., Foulon, R., Marchais, D., Olivier, M.,  
606 D'Ottavi, A., Verzegnassi, F., Mondello, A., Coppola, F., Landi, G., Hoffmann, H.-D.,  
607 Esser, D., Prieto, L.P., Wührer, C., Rivers, C., Bell, R. (2023). Status of Aeolus-2 mission  
608 pre-development activities. Proc. SPIE 12777, *International Conference on Space Optics*  
609 — ICSO 2022, 1277709. <https://doi.org/10.1117/12.2688794>

610 Hersbach, H., Bell, B., Berrisford, P., Biavati, G., Horányi, A., Muñoz Sabater, J., Nicolas, J.,  
611 Peubey, C., Radu, R., Rozum, I., Schepers, D., Simmons, A., Soci, C., Dee, D., Thépaut,  
612 J.-N. (2023). ERA5 hourly data on pressure levels from 1940 to present. Copernicus  
613 Climate Change Service (C3S) Climate Data Store (CDS).  
614 <https://doi.org/10.24381/cds.bd0915c6>

615 Hills, R. C. (1979). The Structure of the Inter-Tropical Convergence Zone in Equatorial Africa and Its  
616 Relationship to East African Rainfall. *Transactions of the Institute of British*  
617 *Geographers*, 4(3), 329–352. <https://doi.org/10.2307/622055>

618 Horányi, A., Cardinali, C., Rennie, M. and Isaksen, L. (2015), The assimilation of horizontal  
619 line-of-sight wind information into the ECMWF data assimilation and forecasting  
620 system. Part I: The assessment of wind impact. *Quarterly Journal of the Royal  
621 Meteorological Society*, 141: 1223-1232. <https://doi.org/10.1002/qj.2430>

622 Inoue, J., Yamazaki, A., Ono, J., Dethloff, K., Maturilli, M., Neuber, R., ... & Yamaguchi, H.  
623 (2015). Additional Arctic observations improve weather and sea-ice forecasts for the  
624 Northern Sea Route. *Scientific Reports*, 5(1), 16868.

625 James, E. P., Benjamin, S. G., & Jamison, B. D. (2020). Commercial-Aircraft-Based  
626 Observations for NWP: Global Coverage, Data Impacts, and COVID-19. *Journal of  
627 Applied Meteorology and Climatology*, 59(11), 1809-1825.  
628 <https://doi.org/10.1175/JAMC-D-20-0010.1>

629 Jiang, Q. (2003). Moist dynamics and orographic precipitation. *Tellus A: Dynamic Meteorology  
630 and Oceanography*, 55:4, 301-316, DOI: [10.3402/tellusa.v55i4.14577](https://doi.org/10.3402/tellusa.v55i4.14577)

631 Joe, P., Melo, S., Burrows, W. R., Casati, B., Crawford, R. W., Deghan, A., Gascon, G., Mariani,  
632 Z., Milbrandt, J., & Strawbridge, K. (2020). The Canadian Arctic Weather Science  
633 Project: Introduction to the Iqaluit Site. *Bulletin of the American Meteorological  
634 Society*, 101(2), E109-E128. <https://doi.org/10.1175/BAMS-D-18-0291.1>

635 Jung, T., Kasper, M. A., Semmler, T., & Serrar, S. (2014). Arctic influence on subseasonal  
636 midlatitude prediction. *Geophysical Research Letters*, 41(10), 3676-3680.

637 Jung, T., Gordon, N. D., Bauer, P., Bromwich, D. H., Chevallier, M., Day, J. J., Dawson, J.,  
638 Doblas-Reyes, F., Fairall, C., Goessling, H. F., Holland, M., Inoue, J., Iversen, T., Klebe,  
639 S., Lemke, P., Losch, M., Makshtas, A., Mills, B., Nurmi, P., Perovich, D., Reid, P.,



640 Renfrew, I. A., Smith, G., Svensson, G., Tolstykh, M., & Yang, Q. (2016). Advancing  
641 Polar Prediction Capabilities on Daily to Seasonal Time Scales. *Bulletin of the American*  
642 *Meteorological Society*, 97(9), 1631-1647. <https://doi.org/10.1175/BAMS-D-14-00246.1>

643 Kim, G., Kim, J. & Cha, DH. (2022) Added value of high-resolution regional climate model in  
644 simulating precipitation based on the changes in kinetic energy. *Geosci. Lett.* **9**, 38.  
645 <https://doi.org/10.1186/s40562-022-00247-6>

646 Kiriakidis, P., Gkikas, A., Papangelis, G., Christoudias, T., Kushta, J., Proestakis, E., Kampouri,  
647 A., Marinou, E., Drakaki, E., Benedetti, A., Rennie, M., Retscher, C., Straume, A. G.,  
648 Dandocsi, A., Sciare, J., and Amiridis, V. (2023). The impact of using assimilated Aeolus  
649 wind data on regional WRF-Chem dust simulations. *Atmos. Chem. Phys.*, 23, 4391–4417.  
650 <https://doi.org/10.5194/acp-23-4391-2023>

651 Laroche, S. & Poan, E.D. (2021). Impact of the Arctic observing systems on the ECCO global  
652 weather forecasts. *Quarterly Journal of the Royal Meteorological*  
653 *Society*, 148(742), 252–271. <https://doi.org/10.1002/qj.4203>

654 Laroche, S. & St-James, J. (2022) Impact of the Aeolus Level-2B horizontal line-of-sight winds  
655 in the Environment and Climate Change Canada global forecast system. *Quarterly*  
656 *Journal of the Royal Meteorological Society*, 148(745), 2047–2062.  
657 <https://doi.org/10.1002/qj.4300>

658 Lawrence, H, Bormann, N, Sandu, I, Day, J, Farnan, J, Bauer, P. (2019). Use and impact of  
659 Arctic observations in the ECMWF Numerical Weather Prediction system. *Quarterly*  
660 *Journal of the Royal Meteorological Society*, 145: 3432–3454.  
661 <https://doi.org/10.1002/qj.3628>

662 Lawrence, Z. D., Perlwitz, J., Butler, A. H., Manney, G. L., Newman, P. A., Lee, S. H., & Nash,  
663 E. R. (2020). The remarkably strong Arctic stratospheric polar vortex of winter 2020:  
664 Links to record-breaking Arctic Oscillation and ozone loss. *Journal of Geophysical*  
665 *Research: Atmospheres*, 125, e2020JD033271. <https://doi.org/10.1029/2020JD033271>

666 Le Marshall, J., Jung, J., Zapotocny, T., Redder, C., Dunn, M., Daniels, J., & Riishojgaard, L. P.  
667 (2008). Impact of MODIS atmospheric motion vectors on a global NWP system.  
668 *Australian Meteorological Magazine*, 57, 45–51.

669 Liu, B., Guo, J., Gong, W., Shi, L., Zhang, Y., & Ma, Y. (2020). Characteristics and performance  
670 of wind profiles as observed by the radar wind profiler network of China. *Atmospheric*  
671 *Measurement Techniques*, 13(8), 4589-4600.

672 Martinez, C., Goddard, L., Kushnir, Y. *et al.* (2019). Seasonal climatology and dynamical  
673 mechanisms of rainfall in the Caribbean. *Clim Dyn* **53**, 825–846.  
674 <https://doi.org/10.1007/s00382-019-04616-4>

675 Martin, A., Weissmann, M., and Cress, A. (2023). Investigation of links between dynamical  
676 scenarios and particularly high impact of Aeolus on numerical weather prediction (NWP)  
677 forecasts. *Weather Climate Dynamics*, 4, 249–264. [https://doi.org/10.5194/wcd-4-249-](https://doi.org/10.5194/wcd-4-249-2023)  
678 [2023](https://doi.org/10.5194/wcd-4-249-2023)

679 Mattingly, K. S., Ramseyer, C. A., Rosen, J. J., Mote, T. L., and Muthyala, R. (2016), Increasing  
680 water vapor transport to the Greenland Ice Sheet revealed using self-organizing  
681 maps. *Geophys. Res. Lett.*, 43, 9250–9258. <https://doi.org/10.1002/2016GL070424>

682 McTaggart-Cowan, R., Vaillancourt, P. A., Zadra, A., Chamberland, S., Charron, M., Corvec, S.,  
683 *et al.* (2019). Modernization of atmospheric physics parameterization in Canadian

684 NWP. *Journal of Advances in Modeling Earth Systems*, 11, 3593–3635.  
685 <https://doi.org/10.1029/2019MS001781>

686 Mile, M., Azad, R., & Marseille, G.-J. (2022). Assimilation of Aeolus Rayleigh-clear winds  
687 using a footprint operator in AROME-Arctic mesoscale model. *Geophysical Research*  
688 *Letters*, 49, e2021GL097615. <https://doi.org/10.1029/2021GL097615>

689 Misra, V., DiNapoli, S., & Powell, M. (2013). The Track Integrated Kinetic Energy of Atlantic  
690 Tropical Cyclones. *Monthly Weather Review*, 141(7), 2383-2389.  
691 <https://doi.org/10.1175/MWR-D-12-00349.1>

692 Mizyak, V. G., Shlyaeva, A. V., & Tolstykh, M. A. (2016). Using satellite-derived Atmospheric  
693 Motion Vector (AMV) observations in the ensemble data assimilation system. *Russian*  
694 *Meteorology and Hydrology*, 41, 439-446. <https://doi.org/10.3103/S1068373916060091>

695 Naakka, T., Nygård, T., Tjernström, M., Vihma, T., Pirazzini, R., & Brooks, I. M. (2019). The  
696 impact of radiosounding observations on numerical weather prediction analyses in the  
697 Arctic. *Geophysical Research Letters*, 46, 8527–8535.  
698 <https://doi.org/10.1029/2019GL083332>

699 Olaguera, L.M.P., Caballar, M.E., De Mata, J.C. *et al.* (2021). Synoptic conditions and potential  
700 causes of the extreme heavy rainfall event of January 2009 over Mindanao Island,  
701 Philippines. *Nat Hazards* **109**, 2601–2620. <https://doi.org/10.1007/s11069-021-04934-z>

702 Overland, J., Francis, J. A., Hall, R., Hanna, E., Kim, S., & Vihma, T. (2015). The Melting  
703 Arctic and Midlatitude Weather Patterns: Are They Connected?. *Journal of*  
704 *Climate*, 28(20), 7917-7932. <https://doi.org/10.1175/JCLI-D-14-00822.1>

705 Palmén, E. (1958), Vertical Circulation and Release of Kinetic Energy during the Development  
706 of Hurricane Hazel into an Extratropical Storm. *Tellus*, 10: 1-23.  
707 <https://doi.org/10.1111/j.2153-3490.1958.tb01982.x>

708 Pourret, V., Šavli, M., Mahfouf, J.-F., Raspaud, D., Doerenbecher, A., Bénichou, H., et al.  
709 (2022) Operational assimilation of Aeolus winds in the Météo-France global NWP model  
710 ARPEGE. *Quarterly Journal of the Royal Meteorological Society*, 148(747), 2652–2671.  
711 <https://doi.org/10.1002/qj.4329>

712 Radić, V., Cannon, A. J., Menounos, B., and Gi, N. (2015), Future changes in autumn  
713 atmospheric river events in British Columbia, Canada, as projected by CMIP5 global  
714 climate models. *J. Geophys. Res. Atmos.*, 120, 9279–9302.  
715 <https://doi.org/10.1002/2015JD023279>

716 Randriamampianina, R., Bormann, N., Køltzow, M. A., Lawrence, H., Sandu, I., & Wang, Z. Q.  
717 (2021). Relative impact of observations on a regional Arctic numerical weather  
718 prediction system. *Quarterly Journal of the Royal Meteorological Society*, 147(737),  
719 2212-2232.

720 Randriamampianina, R., Schyberg, H., & Mile, M. (2019). Observing System Experiments with  
721 an Arctic Mesoscale Numerical Weather Prediction Model. *Remote Sensing*, 11(8), 981.  
722 <https://doi.org/10.3390/rs11080981>

723 Rani, S. I., Sharma, P., George, J. P., & Das Gupta, M. (2021). Assimilation of individual  
724 components of radiosonde winds: An investigation to assess the impact of single-  
725 component winds from space-borne measurements on NWP. *Journal of Earth System*  
726 *Science*, 130(2), 89.

727 Rennie, M.P., Isaksen, L., Weiler, F., de Kloe, J., Kanitz, T. & Reitebuch, O. (2021). The impact  
728 of Aeolus wind retrievals on ECMWF global weather forecasts. *Quarterly Journal of the*  
729 *Royal Meteorological Society*, 147(740), 3555–3586. <https://doi.org/10.1002/qj.4142>

730 Reynolds, C. A., Crawford, W., Huang, A., Barton, N., Janiga, M. A., McLay, J., Flatau, M.,  
731 Frolov, S., & Rowley, C. (2022). Analysis of Integrated Vapor Transport Biases. *Monthly*  
732 *Weather Review*, 150(5), 1097-1113. <https://doi.org/10.1175/MWR-D-21-0198.1>

733 Smith, G. C., Bélanger, J., Roy, F., Pellerin, P., Ritchie, H., Onu, K., Roch, M., Zadra, A., Colan,  
734 D. S., Winter, B., Fontecilla, J., & Deacu, D. (2018). Impact of Coupling with an Ice–  
735 Ocean Model on Global Medium-Range NWP Forecast Skill. *Monthly Weather*  
736 *Review*, 146(4), 1157-1180. <https://doi.org/10.1175/MWR-D-17-0157.1>

737 Tan, X., Gan, T.Y., & Chen, Y.D. (2019). Synoptic moisture pathways associated with mean and  
738 extreme precipitation over Canada for summer and fall. *Clim Dyn* **52**, 2959–2979.  
739 <https://doi.org/10.1007/s00382-018-4300-6>

740 Velden, C. S., Hayden, C. M., Nieman, S. J., Menzel, W. P., Wanzong, S., & Goerss, J. S.  
741 (1997). Upper-tropospheric winds derived from geostationary satellite water vapor  
742 observations. *Bulletin of the American Meteorological Society*, 78, 173–195.  
743 [https://doi.org/10.1175/1520-0477\(1997\)078,0173:UTWDFG.2.0.CO;2](https://doi.org/10.1175/1520-0477(1997)078<0173:UTWDFG.2.0.CO;2)

744 Velden, C., Lewis, W. E., Bresky, W., Stettner, D., Daniels, J., & Wanzong, S. (2017).  
745 Assimilation of High-Resolution Satellite-Derived Atmospheric Motion Vectors: Impact  
746 on HWRP Forecasts of Tropical Cyclone Track and Intensity. *Monthly Weather Review*,  
747 145, 1107-1125. <https://doi.org/10.1175/MWR-D-16-0229.1>

748 Young, I. R., Sanina, E., & Babanin, A. V. (2017). Calibration and Cross Validation of a Global  
749 Wind and Wave Database of Altimeter, Radiometer, and Scatterometer Measurements.  
750 *Journal of Atmospheric and Oceanic Technology*, 34, 1285-1306.

751 Zuo, H. and Hasager, C. B. (2023). The impact of Aeolus winds on near-surface wind forecasts  
752 over tropical ocean and high-latitude regions. *Atmospheric Measurement Technique*, 16,  
753 3901-3913. <https://doi.org/10.5194/amt-16-3901-2023>